WATER RESOURCES RESEARCH, VOL. 34, NO. 10, PAGES 2671–2683, OCTOBER 1998

Eulerian and Lagrangian correlation structures of convective rainstorms

Don R. May
Engineering Department, Fort Lewis College, Durango, Colorado

Pierre Y. Julien
Civil Engineering Department, Colorado State University, Fort Collins

Abstract. The Eulerian and Lagrangian correlation structures of 13 convective rainstorms were investigated using rainfall data from the 1987 Convective Initiation Downburst Experiment in Denver, Colorado. One minute rainfall data were available for two superposed raingage networks: 46 raingages on the portable automated mesonet (PAM) network at a mean spacing of 10.6 km and 31 additional raingages on the Federal Aviation Administration Lincoln Laboratory Operational Weather Studies (FLOWS) network at a mean spacing of 2.4 km. Eulerian correlation coefficients are low and often negative for high-resolution 1 min rainfall data. Correlation increases with time-averaging, beyond 10–15 min for single rain cells on the FLOWS network and small-mesoscale rainstorms on the PAM network. The average speed of rain cells and small-mesoscale rainstorms was found to be 76.5 and 56.4 km hr^{-1}, respectively. Storm kinematic is identified as the cause of data scatter and low Eulerian correlations. Convective rainstorms are essentially uncorrelated in the Eulerian reference frame at a typical raingage spacing of 2–3 km for rain cells and 10–15 km for small mesoscale rainstorms. A spatial cross-correlation analysis in a Lagrangian reference frame moving with the center of mass of the storm separates the kinematic component from the structural component of a rainfall field. The spatial cross correlations in the Lagrangian rainfall field show considerable improvement over the Eulerian spatial correlation plots, and data scatter is greatly reduced. The increase in correlation coefficients from Eulerian to Lagrangian reference frames typically ranged from 0.5 to 1.1.

1. Introduction

The mathematical structure of rainfall events has been examined using point process theory since *Todorovic* [1968] and *Todorovic and Woolhiser* [1974]. A stochastic representation of ground level rainfall intensity in space and time was presented by *Waymire et al.* [1984]. *Rodriguez-Iturbe et al.* [1984] showed that the mathematical description of rainfall process depends on the scale of measurements. *Valdes et al.* [1985] proposed a model representing the temporal structure of a multidimensional rainfall process. The model simulates moving storms with mesoscale meteorological features including clustering, birth, and death of rain cells and cell intensity attenuation in space and time. *Rodriguez-Iturbe and Eagleson* [1987] investigated rainfall from storm events using point process techniques. Accordingly, cells are distributed in space either independently following a Poisson process or with clustering according to a Neyman-Scott scheme. Multidimensional models of nonstationary space-time rainfall have been developed by *Sivapalan and Wood* [1987] in which a storm is assumed to consist of a hierarchy of scales of which the rain cells are embedded within small mesoscale areas, which are then embedded within large-mesoscale areas. Several methods based on multiscaling and self-similarity ideas have been proposed in recent years and a multicomponent decomposition of spatial rainfall fields are given by *Kumar and Foufoula-Georgiou* [1993a, b]. The effects of radar rainfall resolution on surface runoff calculation were examined by *Ogden and Julien* [1994], showing that the correlation length of radar rainfall precipitation was of the order of 2–3 km. The practical lower-limit resolution for weather radars was found to be of the order of 1 km for unbiased surface runoff calculations. The foregoing analysis focuses on the correlation structure of rainfall measurements from large networks of raingages.

Ground-based raingage networks supply a reliable source of precipitation data used in statistical analyses associated with the development of rainfall models and the calibration of radar estimates of rainfall. For years, various correlation techniques have been used to evaluate both the temporal and spatial structure of rainfall events [*Boyer*, 1957; *Berndtsson*, 1972]. A study by *Felgate and Read* [1975] demonstrated the potential for correlation techniques to accurately describe the small-scale structure of rainstorms in quantitative terms. Using a network of 16 gages at 1 km spacing, they were able to determine the spatial scale, mean lifetime, and velocity of rainfall cells. *Drufuca and Zawadski* [1975] evaluated 10 years of raingage data from a single site for numerous statistical measures including the autocorrelation function and the probabilities of various rainfall rates. They proposed the notion that the variability in a gage measured rainfall pattern arises from two effects: (1) advection of the spatial rainfall pattern and (2) changes that occur as the pattern moves over the gage. *Zawadski* [1973] measured space and time autocorrelation functions

Paper number 98WR01531.
0043-1397/98/98WR-01531$09.00

for the rainfall process on a horizontal plane. He determined the structure and motion of the storm and differentiated between convective cell motion and storm motion.

Marshall [1980] performed a cross-correlation analysis at different time lags between all pairs of gages for storms passing over two networks in England. Both networks were at the cell scale and covered ~25 km^2. One network had 16 gages, and the other had 36. His results gave an indication of the temporal and spatial structure of the storms analyzed. He used a frame of reference which moves with the rainfall feature and the autocorrelation function to indicate the rate of change of moving rainfall patterns. In conclusion, Marshall was able to use correlation surfaces to determine the shape, orientation, and rate of decay of convective cells as well as their kinematic properties.

Shaw [1983] performed both autocorrelation and cross-correlation analyses in evaluating the cellular structure of storms. He performed these analyses on groups of three gages at a time. He delineated characteristic ellipses representative of the 0.5 correlation contour and then used the size of this ellipse as a measure of the cell size. Shaw was also able to obtain an estimate for the mean lifetime of storm cells.

A cross-correlation analysis by *Messaoud and Pointin* [1990] was used to determine the minimum time interval and spatial gage resolution for which statistically significant results can be obtained. Their study included a comparison of data from both a gaged network and a weather radar for the same event. They found that the cross-correlation coefficient between pairs of stations decreased as the gage separation distance increased. In addition, they found that for time intervals <15 min the mean rainfall rate for a single gage is not statistically representative of a mean value over the area that the gage is supposed to cover.

May and Julien [1990] found similar results using a cross-correlation analysis of 1 min rainfall data from a 30 raingage network. The use of spatially fixed raingages as a tool to measure the very dynamic nature of rainfall events suggests that resulting rainfall records may be more complicated than originally thought. Raingages operate in the Eulerian reference frame, and Eulerian spatial correlations make perfect sense for stationary rainstorms. The correlation structure is, however, expected to deteriorate as the speed of moving rainstorms increases. In fact, when the rainfall ceases at a given raingage, one cannot determine whether rainfall ceased over the entire cell or whether the storm moved outside of the raingage network. One expects a stationary rainstorm to be better represented by the Eulerian rainfall data than a moving rainstorm. As the speed and rate of deformation of the rain cells increase, the results of traditional analyses in the Eulerian reference frame are less likely to be meaningful. The frame of reference which moves with the rainfall cell is termed the Lagrangian reference frame and forms the basis for the method presented in this paper.

2. Objectives

A Lagrangian transformation based on the hypothesis that the observed variations in a rainfall event moving over a network can be substantially attributed to two quasi-independent and distinct processes: (1) rain cell kinematics and (2) and rain cell structure. Ideally, the true nature of rainfall fields, represented by data collected from raingage networks, would be better modeled if the structural and kinematic components were considered separately. One may assume that the atmospheric mechanism which controls storm speed is independent of the mechanisms which controls rainfall intensity, duration, and geometry of a rain cell. If this hypothesis is true, a statistical picture of the data after Lagrangian transformation should be clearer than a picture of the data prior to the transformation.

The objective of this study is to examine the correlation structure of several convective rainstorms after a Lagrangian transformation moving with the center of mass of a rain cell. It is intended to examine whether or not the correlation structure improves after Lagrangian transformation. The specific objectives of this study are to (1) examine the Eulerian correlation structure of several convective rainstorms measured from two superposed raingage networks; (2) examine rainstorm kinematics of several events in terms of storm speed and direction with raingage network data; and (3) determine the Lagrangian rainfall field and compare the Lagrangian correlation structure with the Eulerian correlation structure for the same rainstorms. Data used in this study were collected from the portable automated mesonet (PAM) and Federal Aviation Administration Lincoln Laboratory Operational Weather Studies (FLOWS) automated mesonet stations associated with the Convective Initiation Downburst Experiments held in Denver, Colorado during the summer of 1987 [*Kessinger*, 1987].

3. Cinde Field Experiment: Rainfall Data

During the summer of 1987 a joint field program entitled the Convection Initiation Downburst Experiment (CINDE) was conducted in the Denver area by a number of agencies and universities. The purpose of the CINDE project was (1) to investigate the kinematic and thermodynamic structures of boundary layer convergence lines that lead to the initiation of storms, (2) to investigate the structure and evolution of the mesoscale boundary layer, and (3) to study processes which lead to microburst downdrafts [*Kessinger*, 1987].

Numerous atmospheric measurement systems were incorporated in the experiment including 31 Federal Aviation Administration (FAA)-Lincoln Laboratory Operational Weather Studies (FLOWS) automatic weather stations and 46 National Center for Atmospheric Research (NCAR) portable automated mesonet (PAM) II stations. These instruments measure a suite of climatologic variables including the 1 min rainfall depth analyzed in this study. *Kessinger* [1987] and *Wolfson* [1989] provide detailed descriptions of the PAM and FLOWS instrumentation. The locations of the PAM and FLOWS raingages are shown in Figure 1.

A summary of the spatial and temporal characteristics of the PAM and FLOWS networks is given in Table 1. Data quality and compatibility between networks were evaluated using several measures. *May* [1993] found that on the basis of close comparison of the cumulative rainfall depths between collocated stations the PAM and FLOWS data were sufficiently free of instrumental bias to allow direct intercomparison between data derived from these networks. It was further found that the use of 1 min data should be restricted to analyses where timing is not critical. In general, 2 min or greater time averages should be used. Table 2 shows the scale properties, equivalent diameter, and duration of 13 rainstorm events used in this analysis. The scale classification is based on *Orlanski*'s [1975] taxonomy of meteorologic features. Nearly all storms used in this study were convective. The FLOWS network monitored rain cells

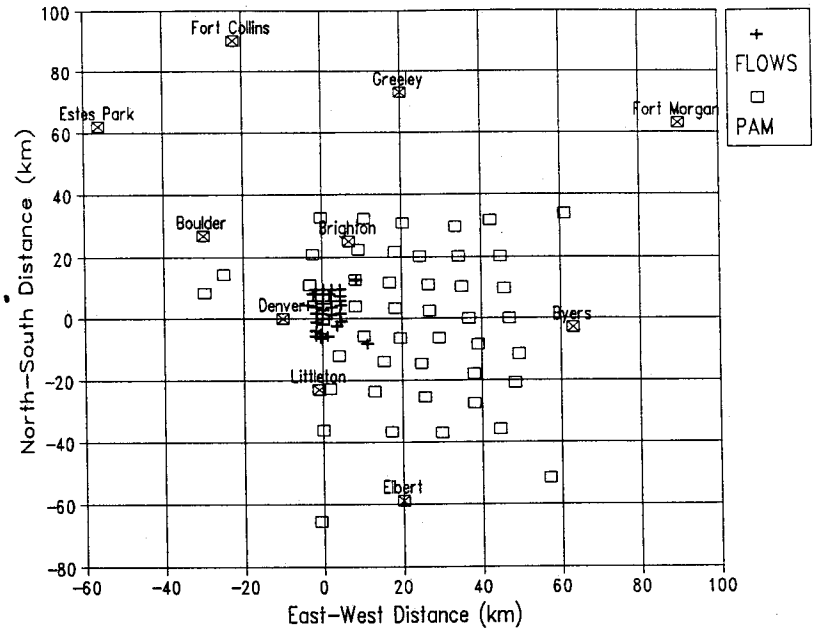

Figure 1. Raingage locations for the portable automated mesonet (PAM) and Federal Aviation Administration Lincoln Laboratory Operational Weather Studies (FLOWS) networks. The origin is at the CP-3 radar location.

and clusters. The PAM network monitored large cell clusters and small-mesoscale rainstorms.

4. Eulerian Correlation Structure of Rainstorms

The correlation coefficient is a measure of the dependency, or predictability, between two time series. It can be used to characterize the structure of a rainfall process represented by the measured time series from two raingages of a network. Spatial correlation graphs display values of the correlation coefficient against the separation distance between two raingages. Normally, stations in close proximity should be highly correlated, while stations far apart should be poorly correlated or uncorrelated. The rate of change of the spatial correlation curve is a function of the size and type of rain cell being analyzed. In the case of convective rain cells, once the separation distance is greater than the cell size, any correlation is due to background rainfall common to all local cells and is attributed to larger-scale features.

4.1. Cross-Correlation Algorithm

Simultaneous and time-lagged serial correlations give information about the temporal structure of an event. In a similar manner the spatial structure of rainfall events is evaluated using time-lagged cross correlations between the time series from pairs of raingages at different spatial locations. The variable of interest in this time series analysis is the rainfall depth $r(G,t)$, occurring during time period t at position G. The general form of the equation used to compute the cross-correlation coefficient ρ is

$$\rho_\tau(G_i,G_j) = \frac{1}{n_\tau} \frac{\sum_{k=1}^{n} [r(G_i,t_k)\delta_k - \bar{r}(G_i)][r(G_j,t_k+\tau)\delta_k - \bar{r}(G_j)]}{S(G_i)S(G_j)} \quad (1)$$

where $\rho_\tau(G_i, G_j)$ is the correlation coefficient between the time series at stations G_i and G_j at lag time τ, n_τ is the number of values from the lagged series used in the computation of ρ, δ_k is a joint rainfall indicator defined below, $\bar{r}$ is the mean for the series, and S is the biased estimate of the standard deviation.

In order to avoid artificially increasing ρ because of extended periods without rain the joint rain indicator δ_k used by *Messaoud and Pointin* [1990] is defined as

$$\delta_k = \begin{cases} 0, & \text{if } r(G_i,t_k) = r(G_j,t_k+\tau) = 0 \\ 0, & \text{if } t_k < t_0 \text{ or } (t_k+\tau) > T = t_0 + (n-1)\Delta t \\ \text{else } 1 \end{cases} \quad (2)$$

where T is the event duration, Δt is the time step, and t_0 is the starting time period.

The lag time τ can be positive, negative, or zero. A positive lag between stations G_i and G_j is defined as the rainfall $r(G_i, t)$ occurring at station G_i and time t is correlated with the rainfall $r(G_j, t + \tau)$ occurring at station G_j and time $(t + \tau)$. *McCuen and Snyder* [1986] recommend limiting the magnitude of τ to ~10% of the record length n at a lag of zero. For each

Table 1. Spatial and Temporal Characteristics of the PAM and FLOWS Networks

Characteristic	FLOWS	PAM
Number of stations	30	46
Mean gage spacing, km	2.4	10.6
Areal coverage, km*	8.4 × 15.3	52.4 × 69.6
Time increment, min	1	1

PAM, portable automated mesonet; FLOWS, Federal Aviation Administration Lincoln Laboratory Operational Weather Studies.

*This reflects the dimensions of the clustered array of stations. Seven stations were located outside this area.

Table 2. Kinematic and Scale Properties of CINDE Rainfall Events

	Network	Scale	Equivalent Diameter, km	Duration, min	Speed, km hr^{-1}	Azimuth, deg
6-29B	FLOWS	cluster	7–12	60	40.3	124.5
7-12B	FLOWS	cluster	3–10	65	156.1	137.6
7-29	FLOWS	cell	4–8	30	23.1	331.2
6-29A	PAM	SMSA	20–25	200	91.1	136.0
6-29B	PAM	SMSA	21–36	180	37.5	108.8
7-03a	PAM	cluster/SMSA	20–25	26	87.8	48.3
7-12B	PAM	SMSA	18–24	141	36.4	114.6
7-17	PAM	SMSA	21–31	58	56.3	27.2
7-03b	PAM	cluster/SMSA	20–25	26	15.5	140.1
7-12a	PAM	SMSA	18	102	70.0	132.3
7-12b	FLOWS	cluster	3–10	65	110.2	132.4
6-29a	FLOWS	cell	5–9	16	89.8	143.3
6-29b	FLOWS	cluster	7–12	60	39.4	124.9
Average or range	FLOWS	cells and clusters	3–12	46	76.5	124–331
Average or range	PAM	clusters and SMSAs	18–36	117	56.4	27–136

CINDE, Convection Initiation Downburst Experiment; SMSA, small-mesoscale area.

lag, one observation point is lost. Thus the number of data points used in the correlation computation at any lag τ is equal to

$$n_\tau = n_{\tau=0} - \tau \tag{3}$$

Once τ exceeds this empirical limit (10% of n), the correlogram may begin to oscillate and produce unreliable results.

4.2. Negative Correlation Coefficients

The value of the correlation coefficient for a one-dimensional random variable such as temporal rainfall is directly indicative of the relationship between two time series. Repeated computations for numerous time series reflect the structure of the rainstorm. In the case where the variable is multidimensional, like cross correlations of space-time rainfall, interpretation of the correlation coefficient is not as simple. Two series may exhibit a strong positive dependency in one domain, spatial, for example, but variations in the temporal domain can mask this dependency resulting in a poor or negative correlation. The hypothetical example shown in Figure 2 illustrates this phenomenon. In each of these five graphs the same base time series was assigned to two stations. This is representative of a moving storm cell whose structure is time invariant. The series at station 2 is then progressively lagged in time, and the correlation coefficient is computed. For this specific example the correlation coefficient gradually decreases from 1, 0.63, 0.1, −0.15, and −0.39 as the time lag increases from 0 to 4, respectively. Even though the series are identical in structure and thus spatially highly correlated, time differences result in poor and negative correlations. In nature, time lagging may be caused by rain cell kinematics as will be shown in the Lagrangian correlation analysis.

4.3. Results of Eulerian Correlations

The general form of spatial correlation graphs for the CINDE data set is shown in Figures 3 through 7. Data scatter and low correlation or inverse correlation are prominent features of these plots. Several display the expected decrease in spatial correlation as the gage separation distance increases. The magnitudes of the corresponding correlations are, however, very low or negative.

The FLOWS network is well suited to the description of single convective rain cells with a diameter typically <10 km. Figure 3 illustrates the scatter obtained from 2 min resolution data. There is little to achieve on single cells at such short-time rainfall resolution. Figure 4 is typical of the results obtained for a single convective rain cell. The 1 min rainfall data exhibit very low correlations as in Figure 3 with a decreasing value of the correlation coefficient with raingage spacing. Data aggregation over periods of 5 and 15 min largely improves the correlation structure of single rain cells. For instance, 1 min data that were uncorrelated at a distance of 6 km showed average correlation coefficients as high as 0.7 when the data was aggregated over periods of 15 min. One way to alleviate the effects of moving rainstorms on the correlation structure is to aggregate the data over longer time periods. The values of the correlation coefficient $\rho > 0.6$ for 15 min rainfall data on Figure 4 correspond to separation distances $<\sim 7$ km, which is approximately the equivalent diameter of the convective rain cell given in Table 2 as 4–8 km.

This corroborates the results of a radar rainfall data analysis by *Ogden and Julien* [1994] whereby the correlation length of convective rainstorms at the Colorado State University (CSU) Universities of Chicago and Illinois (CHILL) radar located near Greeley, Colorado, was estimated at 2.3 km for several convective rainstorms. The implications in terms of modeling surface runoff using the model CASC2D developed by *Julien et al.* [1995] are that rainfall precipitation can be assumed to be fairly uniform on watersheds not exceeding ~5 km^2. For large watersheds in this area, i.e., exceeding ~100 km^2, one may assume an uncorrelated rainfall precipitation field for the calculations of surface runoff from convective rainstorms.

Small-mesoscale rainstorms and cell clusters are best analyzed with the PAM raingage network. Short-term 5 min raingage data display low correlation on Figures 5 and 6 for separation distances between raingages from 10 to 100 km. It is very difficult to obtain any substantial correlation with the PAM network because the spacing between raingages is too large. For the same small-mesoscale rainstorms the correlation structure is shown on Figure 7 at raingage spacing <15 km with raingage data varying from 1 to 15 min. The 1 min raingage data display slightly negative correlations, while the 5 min data display slightly positive correlations. Correlation coefficients

exceeding 0.6 are only obtained after time averaging the rainfall data over time intervals exceeding 15 min.

Causes of these unexpected low correlation coefficients obtained for high-resolution 1 min rainfall data were investigated in detail. Two probable explanations were identified:

1. The first and most significant is due to the progressive spatial displacement of rain cells between the raingages. As the rainfall cell moves over a fixed network, raingages collect rainfall from different positions within the cell.

2. The lag time between hyetograph centroids which maximizes the correlation between the time series is different for each pair of raingages in the network. For instance, one would expect high correlation between two adjacent raingages under rain cells of constant and uniform intensity. For fast moving storms, however, this expected correlation is degraded because the time series at any two stations can easily be lagged from one another by several time periods. The principal conclusions obtained from this Eulerian analysis are that (1) high-resolution rainfall data (<5 min) are prone to negative and low correlation coefficients; (2) correlation coefficients are much higher after time-averaging of the rainfall data over periods >10 min; (3) the PAM network with an average raingage spacing of 10 km is suited for small-mesoscale rainstorms but is too sparse for either single rain cells or clusters; and (4) the FLOWS network with an average raingage spacing of 2–3 km is conducive to a satisfactory correlation analysis for cells and clusters when the data is averaged over at least 10 min.

5. Rainstorm Kinematics

Rainstorm kinematics describes both the speed and direction of a rainfall cell. The determination of rainstorm kinematics is an essential component of the forthcoming Lagrangian transformation process. Quantitative estimation of average rainstorm kinematics results in a single vector which represents the average direction and velocity of an entire rainfall cell. The degree to which the average represents a useful estimate of rainstorm kinematics depends on the scale of the cell. An increase in scale is paralleled with an increase in the complexity of the composite motion of the ever-increasing number of smaller cells imbedded within a cluster. As the scale increases, the average becomes a coarser estimate of the kinematics of the aggregate. The analysis of single cells, however, should be straightforward, and rainstorm kinematics can be refined when using shorter time steps.

5.1. Diskin's Model: A Linear Bivariate Scheme

Diskin [1987, 1990] proposed a method for estimating storm kinematics. Accordingly, moving storms are characterized by the fact that the hyetographs at stations along the direction of the storm movement are displaced on the time axis with respect to one another. *Diskin* [1987, 1990] states that the problem can be interpreted geometrically as the determination of the equation of an inclined plane in the x, y, t space, so that it best represents a given data set. In his scheme the maximum slope on the inclined plane is the inverse of the speed, and the direction of the maximum slope is the direction of the storm motion.

The equation of the plane is derived from data sets of (x, y) coordinates of the raingages and the time of arrival of some significant feature of the recorded hyetograph. The results of this study showed that the outcome is critically dependent on the choice of the significant cell. The time of inception of rainfall and the center of mass of the hyetograph are evaluated. Because of the irregularity in setting the onset of rainfall at any one station, this option gave relatively poor results. The use of the center of mass of the hyetograph, on the other hand, has an averaging effect which yields good results.

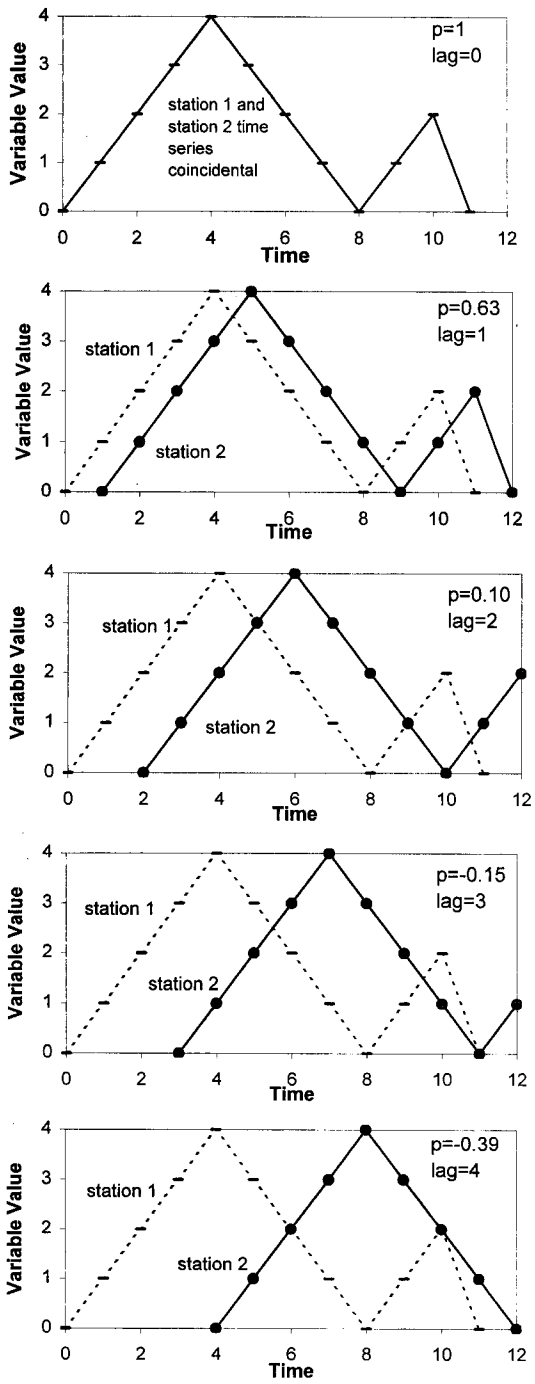

Figure 2. Correlation coefficients for lagged time series: (top) lag = 0 and $\rho = +1$ and (bottom) lag = 4 and $\rho = -0.39$.

5.2. Optimal Fit of Kinematic Parameters

Using the Diskin technique, storm speed and direction are determined by the time of arrival, t, of the center of mass of the hyetograph at a station of known location (x, y). At each

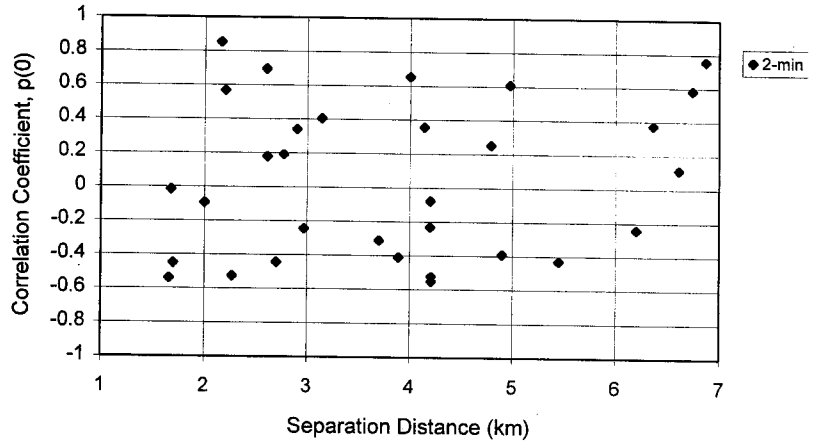

Figure 3. Eulerian correlation versus separation distance for a rain cell (F729a).

raingage the time centroid of the hyetograph of intensity, r_i, over the rainstorm duration T is computed using

$$t = \frac{\int_{t_i}^{T} t_i r_i \, dt}{h_t} = \frac{\sum_{t=t_i}^{T} t_i r_i \, \Delta t}{h_t} \tag{4}$$

$$h_t = \int_0^T r_i \, dt \approx \sum_{t=0}^{T} r_i \, \Delta t \tag{5}$$

where t_i, h_i, and r_i are the time, rainfall depth, and rainfall intensity at time step i, respectively, and h_t is the total rainfall depth under the hyetograph.

Assuming a constant speed and direction throughout the storm, the prediction equation for the time centroid of a rainstorm calculated from (4) for each raingage of known location (x, y) can be defined as

$$t = ax + by + c \tag{6}$$

The parameters a, b, and c in (6) are determined by minimizing the sum of the squared deviations between observed and predicted values of t for all the raingages of a network. A numerical optimization routine was used to accomplish this task. Once the optimized parameters are determined, the speed v and direction θ are found using the following equations:

$$v = \frac{1}{\sqrt{a^2 + b^2}} \tag{7}$$

$$\theta = \tan^{-1}\left(\frac{b}{a}\right) \tag{8}$$

5.3. Results of Rainstorm Kinematics

The events from the PAM and FLOWS networks were used to test this technique. Figure 8 shows several plots of the arrival times of the hyetograph centroid versus distance from the edge of the network for four sample events. This simple bivariate linear relationship proposed by Diskin worked well on the CINDE data. Deviations between the predicted and actual arrival times can be attributed to the nonlinear motion of rainstorms and the incongruent motion of multiple cells within an event. Unusually large discrepancies occur when computed centroidal times spread near the extremities of the network domain. The remaining variations between computed and predicted centroid arrival times can be associated with internal changes in a cell, particularly when clusters form.

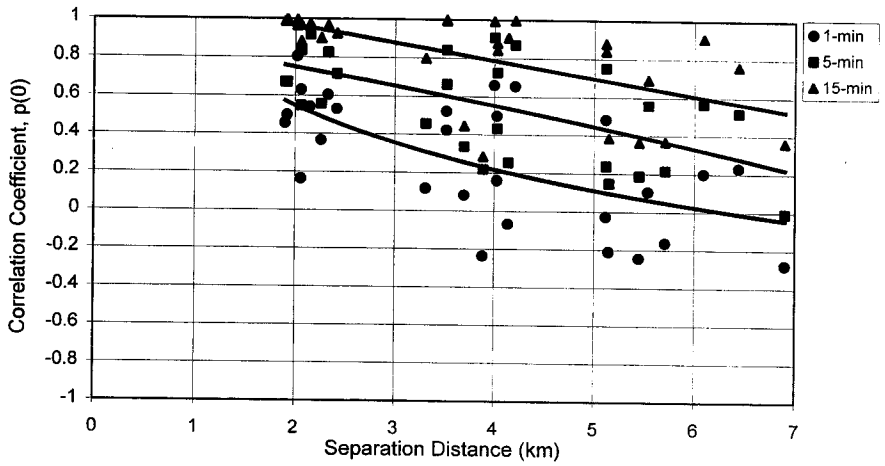

Figure 4. Eulerian correlation versus gage separation distance for a rain cell (F729).

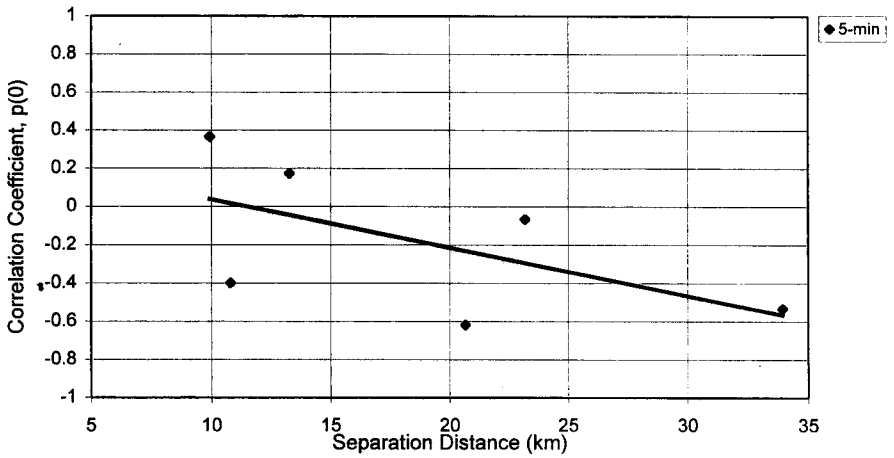

Figure 5. Eulerian correlation coefficient versus gage separation distance for a cell cluster (P703).

It can be seen from the speed and direction data in the last two columns of Table 2 that most storms move to the northeast at speeds ranging from 15 to 156 km hr^{-1}. The average velocity for the FLOWS events is 76.5 km hr^{-1} and for the PAM events is 56.4 km hr^{-1}. For general comparison purposes, *Diskin* [1990] reported a velocity range for convective events in Lund, Sweden, of 59–120 km hr^{-1}. *Marshall* [1980] estimated that 60% of the 230 convective storms he analyzed near Winchcombe, England, had a velocity <54 km hr^{-1}. *Sherman* [1977], working with a data set of convective cells from Cardington, England, computed a mean velocity of 41 km hr^{-1} with a maximum of nearly 120 km hr^{-1}. With reference to the surface runoff simulations using the distributed rainfall-runoff model CASC2D, *Ogden et al.* [1995] found that for a given rain cell, kinematics increases the peak discharge for watersheds draining in the direction of the moving rainstorm when the rainstorm length is less than half the length of runoff. On the eastern slopes of the Colorado Rockies the northeastward storms move in the direction of drainage, and for convective rain storms with an effective size of 10 km the effect on peak surface runoff should be significant on watersheds covering a drainage area exceeding 400 km^2. When comparing identical moving rainstorms on two identical watersheds, one located on the eastern slopes and the other on the western slopes, a lower peak discharge is expected on the western slopes than on the eastern slopes.

6. Lagrangian Correlation Structure

The Eulerian reference frame E is a fixed stationary system from which observations are made. All operational raingage networks measure rainfall in E. In contrast, the Lagrangian reference frame L can be conceptually thought of as attached to and moving with the centroid of rainfall cells. Since a rainfall time series measured with respect to L theoretically exhibits no effect because of storm kinematics, one would expect this series to have a simpler structure or at least to be more representative of the internal structure of rain cells.

Measurement from L is physically impossible with raingage networks; however, the information collected in E contains the L information and thus can be used to generate L fields. The desired outcome of the transformation process is to build a rainfall field $R_L(\alpha, \beta, \tau)$, which is relative to the Lagrangian reference frame, from rainfall data $R_E(x, y, t)$ measured in the Eulerian reference frame. The rainfall field subscripts α, β, τ, and x, y, and t represent the two spatial coordinates of the gages and time for the Lagrangian and Eulerian reference frames, respectively.

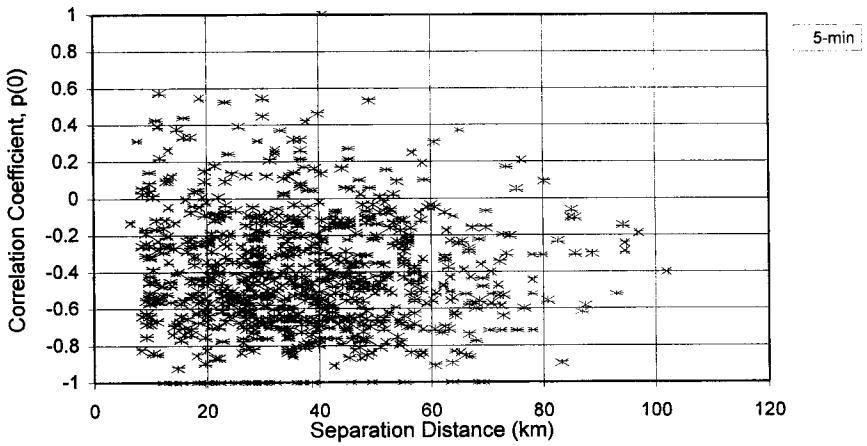

Figure 6. Eulerian correlation versus gage separation distance for a small-mesoscale rainstorm (F629).

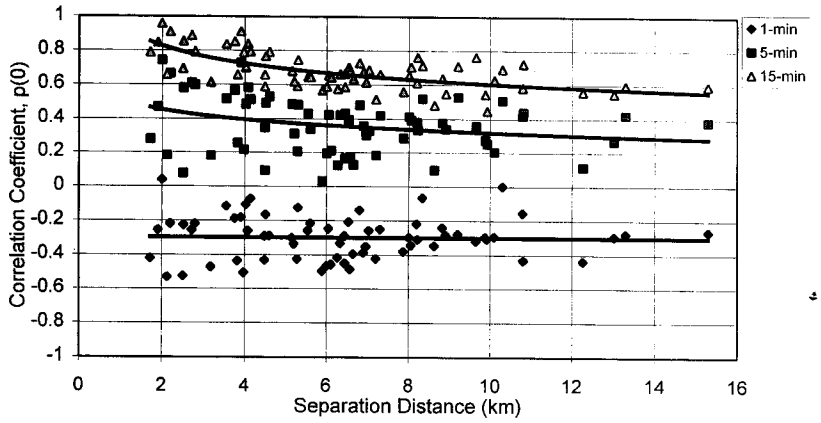

Figure 7. Eulerian correlation versus separation distance for a small-mesoscale rainstorm (F629).

Conversely, a Lagrangian rainfall field (α, β, τ) can be used to construct a rainfall field in E by moving $R_L(\alpha, \beta, \tau)$ over the fixed Eulerian reference frame with a speed and direction representative of the storm from which $R_L(\alpha, \beta, \tau)$ was derived. The resulting field $R_E(x, y, t)$ exhibits the structural variability of $R_L(\alpha, \beta, \tau)$ as well as the kinematic variability introduced by the moving rainfall field $R_L(\alpha, \beta, \tau)$.

The problem of extracting a Lagrangian rainfall field from the measured Eulerian rainfall data set is solved by removing the effects of storm motion from the Eulerian data. This process, termed Lagrangian transformation, is accomplished with the following steps: (1) identify an appropriate rain cell $R_E(x, y, t)$, from the raw data, (2) estimate the cell's kinematic characteristics, for example, using the Diskin model, (3)

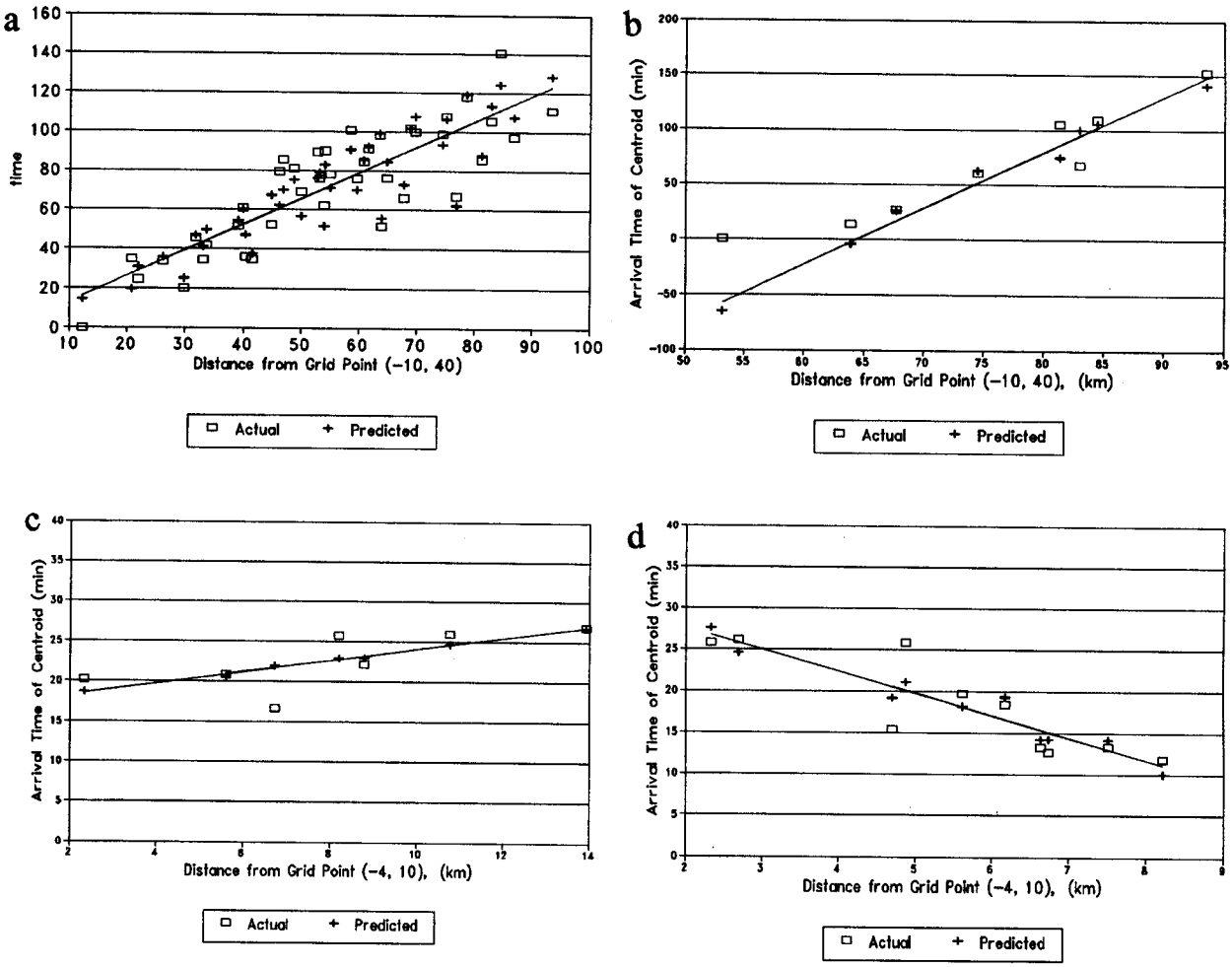

Figure 8. Predicted and computed arrival times for two PAM and two FLOWS rainstorm events: (a) PAM-712YM5 event, (b) PAM-703M2 event, (c) FLOWS-629C2M2 event, and (d) FLOWS-729AM2 event.

increase the density of the E network by interpolating the measured data to a rectangular grid, where the distance between the interpolation nodes is based on the kinematic characteristics of the event, thus resulting in an interpolated rainfall field $R'_E(x, y, t)$, and (4) define the Lagrangian rainfall field $R_L(\alpha, \beta, \tau)$ by moving the initially empty $R_L(\alpha, \beta, \tau)$ over $R'_E(x, y, t)$ and from accumulating rainfall during each time period.

6.1. Densification of the Eulerian Network

A dense Eulerian field is obtained by interpolating rainfall time series at artificial stations located on an equal interval grid. For example, consider a rain cell $R_E(x, y, t)$ described by a measured rainfall data set collected from a network of n nonuniformly spaced gages. Limits on the interpolation grid are defined from delineating the effective area $L_x \times L_y$ from the boundary formed by the outermost gages. The number of interpolation nodes and the grid spacing are determined by the incremental distance the rainfall feature travels during one time period Δt at the computed speed and direction. Specifically, the rainfall feature will move $(\Delta x, \Delta y)$ during one time period. If we let the cell move at angle θ at speed u, then during one period Δt the cell moves a distance $\Delta d = u\Delta t$, or, correspondingly, $\Delta x = u\Delta t$, and $\Delta y = v\Delta t$, where u and v are the x and y components of the rainstorm velocity, respectively. Interpolation at a grid spacing of $(\Delta x, \Delta y)$ results in a denser Eulerian rainfall field $R'_E(x, y, t)$ with $(L_x/\Delta x)\ x\ (L_y/\Delta y)$ stations derived from the measured data at the original n gages.

Many different schemes have been developed for interpolating spatial information. *Creutin and Obled* [1982] evaluated six techniques for their effectiveness in interpolating rainfall data. They found that in general the more sophisticated statistical techniques, such as kriging or optimal interpolation, gave better results than the smoothing techniques such as the Thiessen polygons. They also concluded that the extra computational burden of the more sophisticated methods may not be worth the increased accuracy. Kriging has been successfully applied to rainfall interpolation in other studies by *Lebel et al.* [1987] and *Dong-Jun et al.* [1990]. In this study a kriging routine was used for rainfall interpolation. A development of the kriging theory is given by *Delhomme* [1978].

6.2. Example of Eulerian Densification

In this example, time series from 41 stations of the PAM network (event July 12, 1987) were used to implement the kinematic model and the kriging interpolation routine. The speed of the rainfall feature was determined to be 36 km hr^{-1} at a direction S 65°E. Using the 5 min time period associated with this data and the spatial extent, 60 × 80 km, of the 41 gages resulted in grid spacing parameters of $\Delta x = 2.76$ km and $\Delta y = -1.26$ km. Using these, the gridded network for the P712y event has 22 columns and 63 rows or 1386 interpolated stations. Upon comparison it was found that densified hyetographs $R'_E(x, y, t)$ from the interpolated grid match very closely with the measured hyetographs at the same location.

6.3. Construction of the Lagrangian Rainfall Field

The Lagrangian rainfall field $R_L(\alpha, \beta, \tau)$ can now be extracted from the densified $R'_E(x, y, t)$. Numerically, this means moving an initially empty Lagrangian rainfall network over $R'_E(x, y, t)$ while accumulating rain in $R_L(\alpha, \beta, \tau)$. The Lagrangian rainfall field $R_L(\alpha, \beta, \tau)$ is made up of one rainfall vector for each station and can be represented as

$$R_L(\alpha,\beta,\tau) = [\bar{r}_L(\alpha_1,\beta_1,T), \bar{r}_L(\alpha_2,\beta_2,T), \cdots, \bar{r}_L(\alpha_n,\beta_n,T)] \tag{9}$$

where $\bar{r}_L(\alpha, \beta, T)$ is a rainfall vector at spatial coordinates (α, β), T is the duration in periods of the event in L, n is the number of stations in the L network. The vector $\bar{r}_L(\alpha, \beta, T)$ can be expressed relative to the Eulerian reference frame E given the following algorithm

$$\begin{aligned}\bar{r}_L(\alpha,\beta,T) = \{&r_E(x_0,y_0,t_1),\ r_E(x_0 + \Delta x, y_0 + \Delta y, t_2),\\ &r_E(x_0 + 2\Delta x, y_0 + 2\Delta y, t_3),\\ &\cdots r_E[x_0 + (T-1)\Delta x, y_0 + (T-1)\Delta y, T]\}\end{aligned} \tag{10}$$

where $r_E(x, y, t)$ is the rainfall depth at spatial location (x, y) and time t in the gridded Eulerian reference frame. At $t = 1$ a typical L station is initially positioned over an E gridded station with coordinates (x_0, y_0). At $t = 2$ the L station has moved diagonally to $(x_0 + \Delta x, y_0 + \Delta y)$ where it accumulates its second period of rainfall. In this fashion the L station moves diagonally across the E interpolated network accumulating one period of rainfall from a new E station each time period. When this process is simultaneously carried out for all L stations, the Lagrangian rainfall field $R_L(\alpha, \beta, \tau)$ is constructed, and the Lagrangian transformation process is completed.

6.4. Results of Lagrangian Correlations

A rainfall field in the Lagrangian reference frame is conceptually free of kinematic effects and thus describes the intrinsic structure of rainfall cells. Once the Lagrangian rainfall field has been determined, the Lagrangian correlations are obtained from a direct application of the cross-correlation algorithm in (1) to the Lagrangian rainfall field $R_L(\alpha, \beta, \tau)$. As an example, Figures 9a and 9b show an isohyetal plot and the spatial correlation graph for the same event relative to the Eulerian and Lagrangian reference frames, respectively. The tops of Figures 9a and 9b illustrate a series of isohyetal plots at a grid spacing of 5 km for four period intervals where each period is 2 min long. These plots show the progression of the small mesoscale rainstorm across the network. Note that in Figure 9a the cell is moving slightly to the east but mostly north. This agrees with the computed directional azimuth of 27.2° for this event. Both the structure of the contours and the location of the centroid change with time.

Study of the isohyetal plots in Figure 9b shows that the same event in the Lagrangian reference frame exhibits little or no motion but that the general structure is slightly changing with time. Because the Lagrangian transformation is based on the average cell kinematics, fluctuations around the center of mass occur when the changes during any given time interval are not accurately represented by the average conditions. A close comparison of the structure of the contours shows that both reference frames yield similar but not identical results. This is the expected outcome of the Lagrangian rainfall field which is constructed from the Eulerian network. The spatial correlations are graphed on the bottoms of Figures 9a and 9b. The average correlation for all points in the Eulerian reference frame is poor, i.e., −0.43. The average correlation for the same event in the Lagrangian reference frame increased to +0.69.

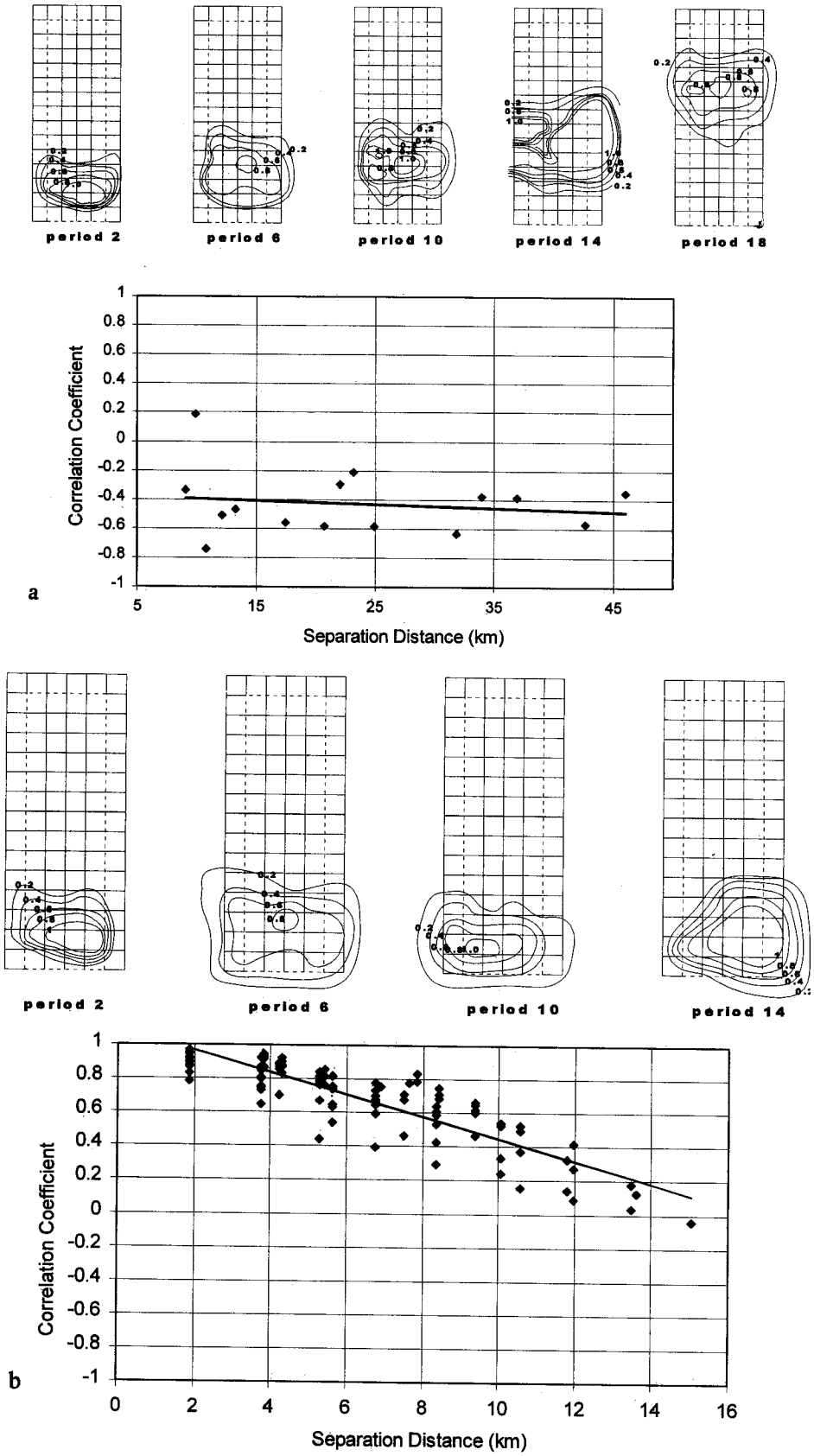

Figure 9. Isohyetal plot of incremental rainfall depth and spatial correlation graph for the PAM (P717) event in the (a) Eulerian and (b) Lagrangian reference frames.

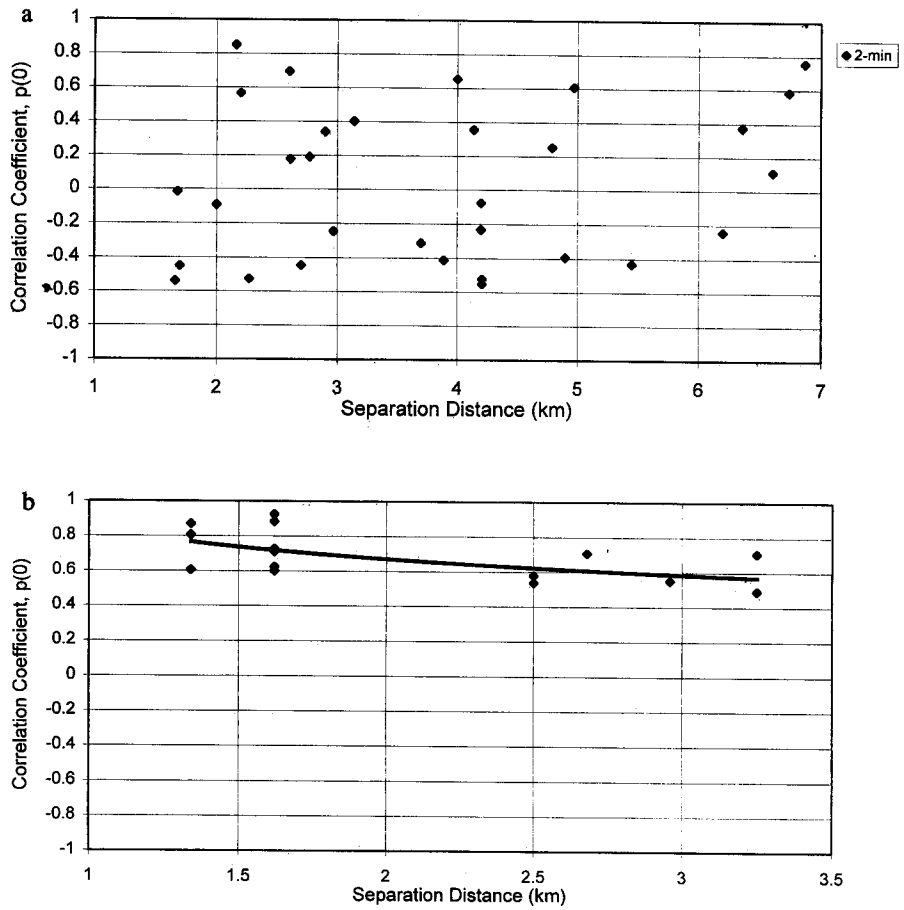

Figure 10. Correlation versus gage separation distance for the FLOWS-729A event.

Numerous rainfall fields constructed in the Lagrangian reference frame tested the effectiveness of the Lagrangian transformation in terms of the degree of spatial correlation obtained in both reference frames. Figures 10 and 11 show the spatial correlation curves for two sample events in the FLOWS and PAM networks, respectively. Figures 10a and 11a show spatial correlations in the Eulerian reference frame with corresponding correlations in the Lagrangian reference frame shown in Figures 10b and 11b. It is evident from these graphs that the level of spatial correlation increased and the amount of data scatter significantly decreased after transformation to the Lagrangian reference frame. The minimum increase in the average correlation coefficient for five test events was 0.53, while the largest increase was 1.11. This is out of a total correlation coefficient range of 2.0 and thus represents increases in average correlation from 25% to over 50%.

The appropriate correlation length that defines the size of convective rainstorms must be determined after the Lagrangian transformation. For instance, it is shown that the intrinsic scale of the rainstorm shown in Figure 9 is ~10–15 km in radius, while the correlation level remains high up to a distance of ~10 km. The equivalent correlation length for the same small-mesoscale rainstorm in the Eulerian reference frame would be much shorter, i.e., 2–3 km.

The implications in terms of hydrologic modeling are that on the basis of the analysis in the Eulerian reference frame one could assume uncorrelated rainfall precipitation fields on large watersheds, for example, in excess of 100 km^2. However, the cross-correlation analysis in the Lagrangian reference frame enables the user to better define (1) the effective size of rainstorms, which is larger than that viewed in the Eulerian reference frame, and (2) the storm kinematics, which can be used to determine whether or not storm kinematics plays a role or not in the peak discharge frame.

To illustrate the effects of storm kinematics, the analysis by *Ogden et al.* [1995] based on two-dimensional surface runoff calculations using CASC2D [*Julien et al.*, 1995] shows that when compared with stationary rainstorms, peak discharge will increase when $0 < (Ut_e/\sqrt{A}) < 5$ and decrease otherwise. The storm speed U is important for rainstorms moving in the direction of drainage depending on the watershed drainage area A and the time to equilibrium t_e. For instance, the time to equilibrium of a complex watershed can be calculated from the method of *Saghafian and Julien* [1995]. For instance, peak surface runoff would be increased on a 900 km^2 watershed with $t_e = 2$ hours for rainstorm velocities $U < 75$ km h^{-1}.

7. Conclusions

This investigation explored the spatial and temporal nature of rainfall events measured in the Eulerian reference frame, i.e., ground-based measured rainfall events. The physical and statistical characteristics of 13 events were determined using an extensive data set from two overlapping networks with a total of 76 raingages.

In the fixed Eulerian reference frame an extensive analysis

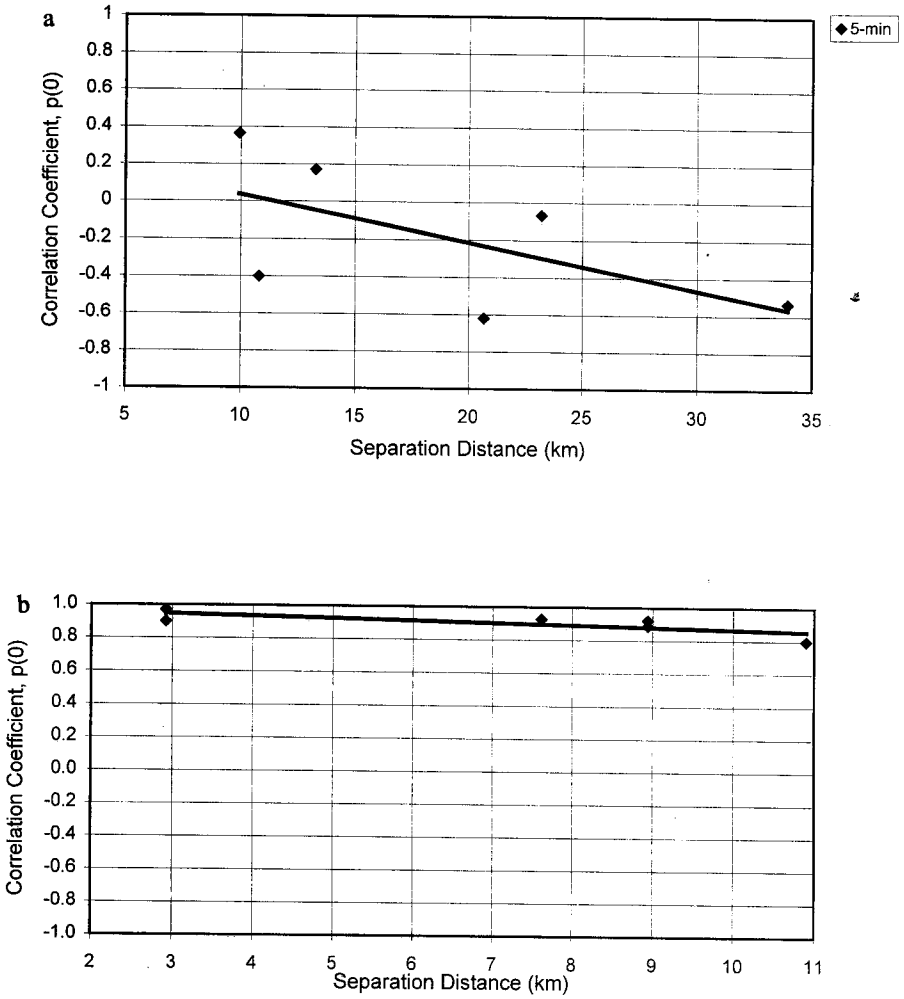

Figure 11. Correlation versus gage separation distance for the PAM-703 event.

using spatial cross correlations showed an obscured statistical picture for both raingage networks. High-resolution data at 1 min intervals give poor correlation and large data scatter. With an average raingage spacing of 2.4 km the FLOWS network yields good correlation coefficients for single cells, clusters, and small-mesoscale events only when the data are aggregated over periods exceeding 10 min. At an average raingage spacing of 10 km the PAM network only yielded good results for small-mesoscale events.

Low Eulerian correlations and large scatter of high-resolution 1 min rainfall data were primarily attributed to storm movement. Rainstorm kinematics cause (1) a progressive spatial displacement between a network of fixed raingages and (2) the lag time between hyetograph centroids which maximizes the correlation between the time series and is different for each pair of gages in the network. These two factors are present in all ground-based network data, but the impact on the correlation structure and other statistics is dependent on the speed of rainstorms. Fair correlations may be obtained for stationary rainstorms. Rain cells and clusters move at an average speed of 76 km h^{-1}, and small-mesoscale rainstorms move at an average speed of 56 km h^{-1}. Storm kinematics cause significant time lag effects for high-resolution 1 min data.

The proposed Lagrangian transformation removes the kinematic effects, significantly increases the average correlation levels, and considerably reduces scatter. The correlation structure in the Lagrangian reference frame better described the internal structure of rainstorms than the Eulerian correlations did. The quality of this description is nevertheless dependent on the spatial and temporal scale of the rainfall data and the ability of the network to accurately capture an event. The Lagrangian transformation is particularly useful for high-resolution rainfall data of moving rainstorm cells, clusters, and small-mesoscale rainstorms. In conclusion, rainfall data collected from raingage networks should be separated into a rainfall structure component and a rainstorm kinematic component prior to statistical analyses and modeling.

Acknowledgments. The authors wish to acknowledge the indirect contributions of F. Ogden, J. Richardson, and B. Saghafian. Special thanks to V. Bringi, V. Chandra, A. Molinas, and F.M. Smith. Assistance in acquiring data was provided by B. Rilling, National Center for Atmospheric Research, Boulder, Colorado. This work was partially sponsored by the U.S. Army Research Office under grants ARO/DAAL 03-86-K-0175 and ARO/DAAH 04-94-G-0420.

References

Berndtsson, R., Temporal variability in spatial correlation of daily rainfall, *Water Resour. Res.*, *24*, 1511–1517, 1972.

Boyer, M. C., Correlation of the characteristics of great storms, *Eos Trans. AGU, 38*, 233–236, 1957.

Creutin, J. D., and C. Obled, Objective analysis and mapping techniques for rainfall fields: An objective comparison, *Water Resour. Res., 18*, 413–431, 1982.

Diskin, M. H., On the determination of the speed of moving rainfall patterns, *J. Hydrol. Sci., 32*, 1–14, 1987.

Diskin, M. H., The speed of two moving rainfall events in Lund, Nord. Hydrol., *21*, 153–164, 1990.

Dong-Jun, S., W. Krajewski, and D. Bowles, Stochastic interpolation of rainfall data from rain gages and radar using cokriging, 1, Design of experiments, *Water Resour. Res., 26*, 469–477, 1990.

Drufuca, G., and I. I. Zawadski, Statistics of raingage data, *J. Appl. Meteorol., 14*, 1419–1429, 1975.

Felgate, D. G., and D. G. Read, Correlation analysis of the cellular structure of storms observed by rain gauges, *J. Hydrol., 24*, 191–200, 1975.

Julien, P. Y., B. Saghafian, and F. L. Ogden, Raster-based hydrologic modeling of spatially-varied surface runoff, *Water Resour. Bull., 31*, 523–536, 1995.

Kessinger, C. (ed.), The CINDE project, operations plan for the convection initiation and downburst experiment (CINDE) near Denver, Colorado, 22 June to 7 August, 1987, Natl. Cent. for Atmos. Res., Natl. Oceanic and Atmos. Admin., Univ. of Wyo., Boulder, Colo., 1987.

Kumar, P., and E. Foufoula-Georgiou, A multicomponent decomposition of spatial rainfall fields, 1, Segregation of large- and small-scale features using wavelet transforms, *Water Resour. Res., 29*, 2515–2532, 1993a.

Kumar, P., and E. Foufoula-Georgiou, A multicomponent decomposition of spatial rainfall fields, 2, Self-similarity in fluctuations, *Water Resour. Res., 29*, 2533–2544, 1993b.

Lebel, T., G. Bastien, C. Obled, and J. D. Creutin, On the accuracy of areal rainfall estimation: A case study, *Water Resour. Res., 23*, 2123–2134, 1987.

Marshall, R. J., The estimation and distribution of storm movement and storm structure using a correlation analysis technique and raingauge data, *J. Hydrol., 48*, 19–39, 1980.

May, D. R., The space-time correlation structure of convective rainstorms in the Lagrangian reference frame, Ph.D. dissertation, Colo. State Univ., Fort Collins, 1993.

May, D. R., and P. Y. Julien, Raingage network resolution with spatial statistics, paper presented at Watershed Planning and Analysis in Action, Am. Soc. of Civ. Eng., Durango, Colo., 1990.

McCuen, R. H., and W. M. Snyder, *Hydrologic Modeling: Statistical Methods and Applications*, Prentice-Hall, Englewood Cliffs, N. J., 1986.

Messaoud, M., and Y. B. Pointin, Small time and space measurements of the mean rainfall rate made by a gage network and by a dual-polarization radar, *J. Appl. Meteorol., 29*, 830–841, 1990.

Ogden, F. L., and P. Y. Julien, Two-dimensional runoff sensitivity to radar resolution, *J. Hydrol., 128*, 1–18, 1994.

Ogden, F. L., J. Richardson, and P. Y. Julien, Similarity in catchment response, 2, Moving rainstorms, *Water Resour. Res., 31*, 1543–1547, 1995.

Orlanski, I., A rational subdivision of scales for atmospheric processes, *Bull. Am. Meteorol. Soc., 6*, 527–530, 1975.

Rodriguez-Iturbe, I., and P. S. Eagleson, Mathematical models of rainstorm events in space and time, *Water Resour. Res., 23*, 191–190, 1987.

Rodriguez-Iturbe, I., V. K. Gupta, and E. Waymire, Scale consideration in the modeling of temporal rainfall, *Water Resour. Res., 20*, 1611–1619, 1984.

Saghafian, B., and P. Y. Julien, 1995, Time to equilibrium for spatially variable watersheds, *J. Hydrol., 172*, 231–245, 1995.

Shaw, S. R., An investigation of the cellular structure of storms using correlation techniques, *J. Hydrol., 62*, 63–79, 1983.

Sherman, R. J., The speed and direction of movement of storm rainfall patterns with reference to urban storm sewer design, Hydrol. Sci. *J., 3*, 421–431, 1977.

Sivapalan, M., and E. F. Wood, A multidimensional model of non-stationary space-time rainfall at the catchment scale, *Water Resour. Res., 23*, 1289–1299, 1987.

Todorovic, P., A mathematical study of precipitation phenomena, *Rep. CER67-68PT65*, Eng. Res. Cent., Colo. State Univ., Fort Collins, 1968.

Todorovic, P., and D. A. Woolhiser, Stochastic model of daily rainfall, paper presented at Symposium on Statistical Hydrology, U.S. Dep. of Agric., Tucson, Ariz., 1974.

Valdes, J. B., I. Rodriguez-Iturbe, and V. K. Gupta, Approximations of temporal rainfall from a multidimensional model, *Water Resour. Res., 21*, 1259–1270, 1985.

Waymire, E., V. K. Gupta, and I. Rodriguez-Iturbe, A spectral theory of rainfall intensity at the meso-β scale, *Water Resour. Res., 20*, 1453–1465, 1984.

Wolfson, M. M., The FLOWS automatic weather station network, *J. Atmos. Oceanic Technol., 6*, 307–326, 1989.

Zawadzki, I. I., Statistical properties of precipitation patterns, *J. Appl. Meteorol., 12*, 459–471, 1973.

P. Y. Julien, Civil Engineering Department, Colorado State University, Fort Collins, CO 80523. (e-mail: pierre@engr.colostate.edu)

D. R. May, Engineering Department, Fort Lewis College, Durango, CO 81301.

(Received May 12, 1997; revised March 27, 1998; accepted May 5, 1998.)